Redox Biology 5 (2015) 195–204

Contents lists available at ScienceDirect

Redox Biology

journal homepage: www.elsevier.com/locate/redox

Research paper

Fluorescence labeling of carbonylated lipids and proteins in cells using coumarin-hydrazide

Venukumar Vemula [a,b], Zhixu Ni [a,b], Maria Fedorova [a,b,*]

[a] Faculty of Chemistry and Mineralogy, Institute of Bioanalytical Chemistry, Leipzig, Germany
[b] Center for Biotechnology and Biomedicine, Universität Leipzig, Leipzig, Germany

ARTICLE INFO

Article history:
Received 18 March 2015
Received in revised form
13 April 2015
Accepted 14 April 2015
Available online 23 April 2015

Keywords:
Coumarin-hydrazide
Dinitrophenyl hydrazine
Fluorescence microscopy
Protein and lipid carbonylation
Spatial distribution

ABSTRACT

Carbonylation is a generic term which refers to reactive carbonyl groups present in biomolecules due to oxidative reactions induced by reactive oxygen species. Carbonylated proteins, lipids and nucleic acids have been intensively studied and often associated with onset or progression of oxidative stress related disorders. In order to reveal underlying carbonylation pathways and biological relevance, it is crucial to study their intracellular formation and spatial distribution. Carbonylated species are usually identified and quantified in cell lysates and body fluids after derivatization using specific chemical probes. However, spatial cellular and tissue distribution have been less often investigated. Here, we report coumarin-hydrazide, a fluorescent chemical probe for time- and cost-efficient labeling of cellular carbonyls followed by fluorescence microscopy to evaluate their intracellular formation both in time and space. The specificity of coumarin-hydrazide was confirmed in time- and dose-dependent experiments using human primary fibroblasts stressed with paraquat and compared with conventional DNPH-based immunocytochemistry. Both techniques stained carbonylated species accumulated in cytoplasm with strong perinuclear clustering. Using a complimentary array of analytical methods specificity of coumarin-hydrazide probe towards both protein- and lipid-bound carbonyls has been shown. Additionally, co-distribution of carbonylated species and oxidized phospholipids was demonstrated.

Introduction

Oxidative stress (OS) is characterized by increased production of reactive oxygen species (ROS) overwhelming the cellular antioxidant defense [1]. Increased ROS levels result in oxidation of numerous biomolecules including proteins, lipids, nucleic acids and carbohydrates [2]. Continuous exposure to high levels of ROS can be detrimental to cells. Acute or chronic OS is associated with numerous pathophysiological conditions, such as Parkinson's and Alzheimer's diseases, atherosclerosis, heart failure, endothelial dysfunction, and inflammatory disorders. It was estimated that over 200 clinical disorders might be directly or indirectly linked to oxidative stress [3].

A major oxidative modification in different biomolecule classes is carbonylation, which refers to all reactions yielding reactive carbonyl groups in the form of aldehyde, ketone or lactam [3]. Protein carbonylation has been studied the best, as this irreversible post-translational modification is believed to trigger protein aggregation in cells and tissues and thus is a well-accepted biomarker of OS-related disorders [4–10]. However, protein carbonylation covers a wide range of chemical modifications. There are multiple mechanisms yielding protein carbonyls and at least three different pathways have been described: (i) metal catalyzed oxidation, (ii) advanced glycation end products, and (iii) reaction with reactive lipid peroxidation products [11]. Reactive lipid peroxidation products carrying carbonyl functions are not only a common source of protein-bound carbonyl, but can also represent an important pool of carbonylated species themselves. Lipid-bound carbonyls have been less studied than protein carbonyls. Nevertheless, several studies demonstrated their importance as a source of protein adducts, immuno-modulating and pro-inflammatory molecules [12]. Truncated carbonylated phosphatidylcholine lipids can be recognized by scavenger receptors leading to induction of immune response and adhesion of monocytes to endothelial cells [12]. Thus in order to understand multiple pathways of biomolecule carbonylation and their biological relevance, it is crucial to follow the distribution of carbonylated species in biological systems.

Carbonylated biomolecules cannot be specifically detected due to the absence of specific physico-chemical properties, such as absorption or fluorescence. Most analytical techniques rely on a

* Correspondence to: Institut für Bioanalytishe Chemie, Biothechologisch-Biomedizinisches Zentrum, Fakultät für Chemie und Mineralogie, Universität Leipzig, DeutscherPlatz 5, 04103 Leipzig, Germany.
E-mail address: maria.fedorova@bbz.uni-leipzig.de (M. Fedorova).

http://dx.doi.org/10.1016/j.redox.2015.04.006

specific chemical derivatization of carbonyl groups with hydrazines, hydrazides and hydroxylamines [3,13]. Derivatized compounds can be detected by absorbance [14], ELISA [15], Western blot [16], chromatography [17], mass spectrometry [18,19] and fluorescence [20–23]. Most of the protocols allow detection or/and quantification of carbonylated species. However, spatial cellular and tissue carbonyl distribution is much less investigated. Carbonylation is a dynamic modification, which tends to accumulate under OS and cellular localization of carbonylated species might change over time. Thus it is important to understand carbonyl spatial dynamic and attribute carbonyl levels to certain molecular species.

One of the most widely used derivatization reagent is 2,4-dinitrophenylhydrazine (DNPH), originally used for spectrophotometric detection and quantification of carbonylated proteins [14]. Availability of anti-DNP antibodies allowed to translate it into sensitive immunodetection by western blots or ELISA [14,15]. Additionally, immunocytochemical detection and fluorescence microscopy imaging was used to evaluate spatial distribution of carbonylated proteins [23–26]. However, standard immunochemistry protocols are time consuming, expensive and often suffer from cross-reactivities of antibodies (Ab). Additionally, DNPH-based immunochemistry protocols are relatively specific for protein-bound carbonyls and thus do not stain other carbonylated biomolecules [23–25].

Here we present a simple, fast and cost efficient microscopy imaging of cellular carbonyls based on coumarin-hydrazide, which provides spatial information on both protein and lipid carbonyls. The protocol was verified for cellular model of paraquat induced OS and compared with DNPH-based immunocytochemistry. Specificity of coumarin-hydrazide was confirmed by gel electrophoresis, thin layer chromatography and mass spectrometry, whereas the co-distribution with oxidized lipids was evaluated by confocal microscopy using oxidized phosphatidylcholine specific natural antibodies.

Material and methods

Chemicals

2,4-Dinitrophenyl hydrazine (DNPH), paraquat (PQ), thiourea, 7-(diethylamino)-coumarin-3-carbohydrazide (CHH), Hoechst 33,258 (Hoechst), 2,7-dichlorofluorescin diacetate (DCFDA), tert-butyl methyl ether (MTBE), primary goat anti-DNP Ab and sodium, potassium, and ammonium salts were purchased from Sigma Aldrich GmbH (Taufkirchen, Germany). Formic acid was obtained from BiosolveBV (Valkenswaard, Netherlands). Dithiothreitol (DTT), urea, and ethanol were obtained from CarlRoth GmbH & Co. KG and chloroform was from Merck KGaA (Darmstadt, Germany). Dulbecco's modified Eagle's medium (DMEM/Ham's F12), fetal bovine serum (FBS), phosphate buffer saline (PBS), 7-aminoactinomysin-D (7-AAD), Trypan Blue (0.1%) and antibiotic (penicillin/streptomycin) solutions were obtained from Life Technologies GmbH (Darmstadt, Germany). Secondary rhodamine (TRITC) AffiniPure Rabbit Anti-Goat IgG (H+L) Ab and peroxidase-conjugated donkey anti-goat Abs were obtained from Jackson ImmunoResearch Laboratories, Inc. (Pennsylvania, United States). E06-monoclonalAb-TopFlour™ antibody was purchased from Avanti Polar Lipids, Inc. (Alabama, United States of America). Low fluorescent PVDF membranes, immunoblot blocking solution (AdvanBlock), immunoblot washing solution (AdvanWash) were purchased from Advansta (California, United States of America).

Cell culture

Human primary skin fibroblasts (kind gift of Dr. Ulf Anderegg, Clinic for Dermatology, Venerology and Allergology, Faculty of Medicine, University of Leipzig) were cultured (37 °C, in a humidified atmosphere of 95% O_2 and 5% CO_2) in DMEM/Ham's F12 medium supplemented with FBS (15%) and antibiotics (1%). Medium was replaced with serum free medium 4 h before paraquat (PQ) was added as solution in DMEM/Ham's F12 (37 °C).

Primary rat cardiomyocytes (Innoprot, Spain) were cultured until 80% confluence in DMEM/F12 medium supplemented with FBS (20%), horse serum (5%), L-glutamine (2 mmol/L), non-essential amino acids (0.1 mmol/L), sodium pyruvate (3 mmol/L) and antibiotics (1%) at 37 °C (95% O_2 and 5% CO_2 atmosphere). Medium was replaced to serum free 24 h prior to 3-morpholinosydnonimine treatment (SIN-1; 10 μmol/L, 30 min).

Primary murine hepatocytes (kind gift of Prof. Dr. Ralf Gebhardt, Institute of Biochemistry, Faculty of Medicine, University of Leipzig) were cultured in William's E medium supplemented with FBS (10%), glutamine (2 mmol/L), antibiotics (0.5%) and dexamethasone (0.1%) at 37 °C (95% O_2 and 5% CO_2 atmosphere). Cells were left to attach for 3 h before medium was replaced with serum free medium containing acetaminophen (10 mmol/L; for 20 h).

DCFDA assay

Cells were grown on flat bottom black 96-well plates (Greiner CELLSTAR®) overnight in DMEM/Ham's F12 medium without FBS. Next day the medium was replaced with transparent DMEM containing DCFDA (10 μmol/L) and incubated (37 °C, 1 h). Cells were washed and incubated in DMEM. After 1 h the medium was changed to DMEM containing different concentrations of PQ and the fluorescence (485/535 nm) was recorded for 3 h on a Paradigm™ Detection Platform (Molecular devices, Salzburg, Austria).

7-(Diethylamino)-coumarin-3-carbohydrazide (CHH) labeling [18,27]

Primary fibroblasts were grown on cover slips. After PQ treatment, cells were washed with PBS, fixed (4% paraformaldehyde, 15 min, 37 °C or ice cold methanol, 10 min, on ice) and washed again (PBS). For CHH labeling cells were blocked in blocking solution (5% FBS, 0.1% Tween-20 in PBS, 1 h, RT) and incubated with CHH (0.2 mmol/L, 2 h, RT). Cells were washed (PBS; 3 times), nuclei were counterstained with 7-AAD (1:300, 30 min, RT), washed (PBS), and the cover slips were mounted on cover slides using Immunoselect Antifading mounting medium (Dianova GmbH, Hamburg, Germany).

For live imaging, after PQ treatment (1 mmol/L, 1 h), cells were washed with warm PBS and incubated with CHH (0.8 mmol/L in DMEM, 2 h, 37 °C). Cells were washed (warm PBS) and imaged immediately.

Immunocytochemistry [23]

Carbonyl compounds were derivatized with DNPH (3 g/L in 98% ethanol containing 1.5% sulfuric acid, 4 °C, overnight on a shaker). Cells were washed thoroughly with washing buffer (1% FBS, v/v, in PBS), and incubated in washing buffer (30 min, 4 °C). Cells were permeabilized (0.5% w/v, Triton X-100, 5 min) and incubated with a goat anti-DNP Ab (1:200 in washing buffer, 1 h, 4 °C). Cells were washed (washing buffer, 3 times), incubated with Rhodamine (TRITC) AffiniPure Rabbit Anti-Goat Ab (1:200 in washing buffer, 1 h, 4 °C) and washed (PBS, 3 times). Nuclei were counterstained with Hoechst Dye (1:1000, 10 min, RT) and washed again (PBS) before the cover slips were mounted on cover slides as described above.

Microscopy

Cells were examined by inverted fluorescent microscope (DMI6000 B, Leica MikrosystemeVertrieb GmbH, Wetzlar, Germany), equipped with an ×40 objective (N. A-0.60), 12 V/100 W halogen lamp as a light source and a Leica DFC360FX camera. Images of DNP labeled carbonyls and 7-(AAD) were acquired with a Cy3/TRITC Filtercube (λ_{exc}=552 nm, λem=578 nm); CHH and Hoechst Dye using with an A4 Filtercube (λ_{exc}=359 nm, λem=461 nm). Images were quantified using ImageJ.

Immunocytochemical detection of oxidized phospholipids

Cells were treated with PQ as described above, incubated in blocking solution (1% BSA in PBS, 1 h, RT) and then with EO6-mAbTopFluor (1:100 in PBS, 1 h, RT) [28,29]. Cells were washed (PBS, 3 times) and the nuclei were counterstained with Hoechst dye. Cells were washed twice with PBS and examined as mentioned above. For co-staining experiments fixed and blocked samples were first incubated with CHH (0.2 mmol/L, 2 h, RT), washed (PBS; 3 times), and stained with EO6-mAbTopFluor (1:100 in PBS, 1 h, RT). Cells were washed (PBS; 3 times), and the cover slips were mounted on cover slides using Immunoselect Antifading mounting medium (Dianova GmbH, Hamburg, Germany). Images for co-localization were obtained with a confocal microscope (LSM 780; Carl Zeiss) equipped with 40 ×/1.3 NA or 63 ×/1.46 NA oil immersion objectives. Image analysis and processing were performed using Zen 2012 Blue software (Carl Zeiss).

Protein extraction

After PQ treatment the medium was discarded, cells were scraped and cell pellets collected by centrifugation (1000*g*, 5 min, 4 °C). Cell pellets were washed (ice cold PBS, 3 times), disrupted in lysis buffer (7 mol/L urea, 2 mol/L thiourea, 2% w/v CHAPS, 50 mmol/L TrisHCl, pH 7.5), and sonicated (20 kHz, 1 min, 30% amplitude; Vibra-Cell, Sonics & Materials, Inc. CT, USA). Samples were centrifuged (10,000*g*, 10 min, 4 °C) and the protein concentration in the supernatant was determined by the Bradford assay.

Western blots

Proteins were dissolved in sample buffer (62.5 mmol/L TrisHCl, pH 6.8, 50 mmol/L DTT, 2% w/v SDS, 20% w/v glycerol, 0.2% w/v bromophenol blue) and separated by SDS-PAGE (10% T; BioRad mini protean III cell; BioRad Laboratories GmbH, München, Germany). Proteins were semidry blotted onto a low fluorescent polyvinylidene difluoride (PVDF) membrane (Trans-Blot Turbo Transfer System, BioRad Laboratories GmbH, München, Germany). Membranes were equilibrated (2 M HCl), derivatized with DNPH (1 g/L in 2 M HCl, 30 min, RT), washed with 2 M HCl (5 min) and methanol (5 min, 5 times). Membranes were blocked overnight (4 °C, Immunoblot Blocking solution; AdvanBlock, Advansta), incubated with goat anti-DNP Ab (1:10,000; in blocking buffer, 1 h, RT), and washed (Immunoblot Washing solution, AdvanWash, Advansta) before peroxidase-conjugated donkey anti-goat Ab (1:10,000, in blocking buffer) were added (1 h, RT). Membranes were visualized using WesternBright Sirius HRP substrate (Advansta) and imaged on a Fusion FX7 Imaging system (Peqlab Biotechnologie GmbH, Erlangen, Germany).

SDS-PAGE of CHH labeled carbonylated proteins

CHH labeled protein pellets remained after lipid extraction were dissolved in lysis buffer and separated by SDS PAGE as described above. CHH derivatized proteins were visualized on a ChemiDoc™ MP (Bio-Rad Laboratories GmbH, München, Germany), using the Image Lab™ software and DyLight 488 channel filter for Blue Epi illumination.

CHH labeling and mass spectrometry analysis of carbonylated lipids

Cell pellets were resuspended in 0.1% aqueous ammonium-acetate (w/v, 50 μL) and derivatized with CHH [18,27]. Briefly, CHH stock solution (3.5 μL,100 mmol/L in DMF) was added to the cell pellet and incubated (1 h, 37 °C). Lipids were extracted using methyl-tert-butyl ether (MTBE) as described previously [30]. Samples were diluted in a mixture of methanol and chloroform (2:1, v/v) containing ammonium formate (5 mmol/L) and analyzed using robotic nanoflow ion source (TriVersaNanoMate; Advion-BioSciences, Ithaca, NY) equipped with nanoelectrospray chip (1.5 kV ionization voltage, 0.4 psi backpressure) coupled to an LTQ Orbitrap XL ETD mass spectrometer (Thermo Fischer Scientific GmbH, Bremen, Germany). The temperature of the transfer capillary was set to 200 °C and the tube lens voltage to 110 V. Mass spectra were acquired with a target mass resolution of 100,000 at *m/z* 400 in a data-dependent acquisition (DDA) mode using FT-MS survey scan followed by consecutive CID fragmentations of the five most abundant ions in the LTQ using gas phase fractionation [27]. Acquired data were analyzed by using Xcalibur software (version 2.0.7).

Thin layer chromatography

CHH-derivatized lipids were separated on HPTLC Silica gel 60 F_{254} plates (7 cm × 10 cm, Merck KGaA, Darmstadt, Germany) using a mixture of dichloromethane and acetonitrile (9:1; v/v). HPTLC plates were dried on air and immediately scanned (Biorad GelDoc EZ Imager, UV Tray; Bio-Rad Laboratories GmbH-Munich, Germany) to visualize carbonylated lipids. All lipid were detected by dipping the plate into primuline solution (0.02% in acetone/water, 8:2, v/v) and imaged (Biorad GelDoc EZ Imager, UV Tray).

Results

Fluorescent microscopy

To induce biomolecules carbonylation in cellular model of primary human fibroblast, paraquat, a well known redox cycling compound, was used. A variety of cellular enzymes (e.g. oxidoreductases such as cytochrome P450) can reduce PQ to the radical cation which is reoxidized by molecular oxygen to PQ with formation of superoxide anion [31,32]. Indeed, over expression of superoxide dismutase (SOD) or treatment with SOD mimetics was shown to reduce PQ-toxicity in a number of studies [33–35]. Superoxide anion in turn can give rise to other ROS formation, including hydrogen peroxide and hydroxyl radical. Large number of studies used PQ as OS inducer in different cellular models [25,36,37]. PQ treatment of primary fibroblast resulted in fast, dose-dependent production of free radicals which was demonstrated by DCFDA assay (Fig. S1). Thus we used this simple cellular model of OS to evaluate CHH labeling of cellular carbonyls.

The specificity of CHH labeling of carbonylated biomolecules was demonstrated with primary fibroblasts treated with PQ (1 mmol/L, 1 h) with and without $NaBH_4$ reduction prior to CHH labeling (Fig. S2). It was clearly demonstrated that reduction of the carbonyl groups with $NaBH_4$ (negative control) diminished the CHH fluorescence.

When cells were incubated with increasing concentrations of PQ (0, 0.25, 0.5, 1, 2 and 5 mmol/L for 3 h), CHH fluorescence

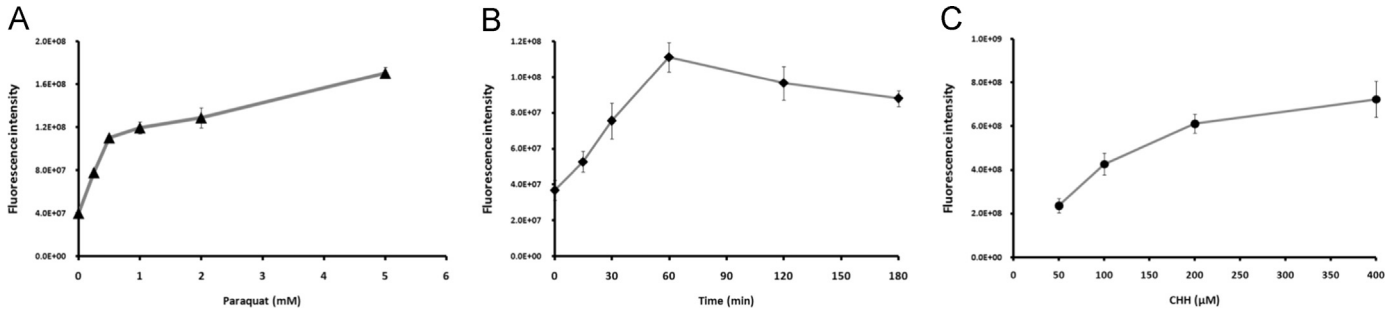

Fig. 1. CHH efficiency to label cellular carbonyls in response to PQ-induced OS. Human primary fibroblasts were treated with different doses of PQ for 3 h (A) or with 1 mmol/L PQ for different time periods (B). The optimal concentration of CHH was evaluated by treating cells with PQ (1 mmol/L) for 1 h (C). Carbonylation levels were evaluated by CHH fluorescence microscopy and images were quantified by ImageJ. The results are expressed as mean fluorescence intensity $\pm$ SD of 15–25 cell images obtained from three independent experiments. Statistical analysis was performed using unpaired *t*-test ($P < 0.0001$ for each conditions versus control).

intensities doubled and tripled at the lowest PQ concentrations compared to the relatively low background that resemble the native carbonylation level of unstressed cells (Fig. 1A). The fluorescence intensity increased gradually afterwards up to the highest PQ dose (5 mmol/L; treatment accompanied by high cell death). Additionally, CHH fluorescence intensity increased with the incubation times (15, 30 min, 1, 2 and 3 h), as indicated for the intermediate PQ concentration (Fig. 1B). The fluorescence increased linearly for 1 h followed by a slight decrease afterwards that is most likely related to the cell death induced by prolonged PQ

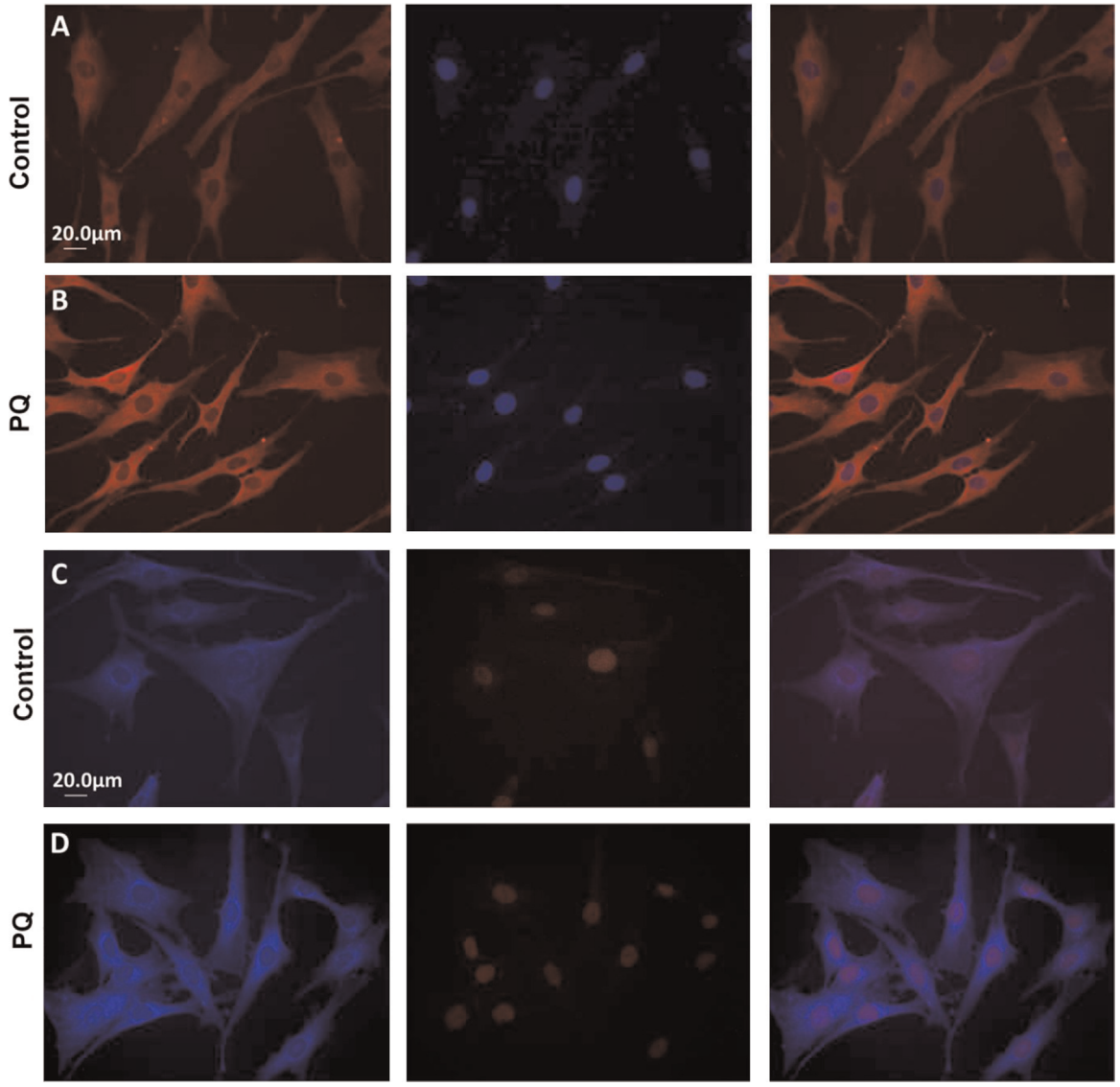

Fig. 2. Fluorescence microscopy of carbonylated biomolecules in PQ-treated primary fibroblasts. Carbonylation was monitored by fluorescence microscopy in control and PQ-treated cells (1 mmol/L, 1 h) using DNPH-based immunocytochemistry (A and B) and CHH labeling (C and D). Images are representatives of three independent experiments performed in triplicates.

treatment. Thus, the CHH fluorescence intensity clearly monitors the dynamic of carbonylation processes in cells.

CHH concentrations up to 200 μmol/L linearly increased the fluorescence intensities (Fig. 1C), whereas a further increase (400 μmol/L) resulted in a higher background, and saturation of the signal intensities in the areas with the highest carbonyl contents. Thus 200 μmol/L CHH was used for all following labeling experiments. Finally, CHH labeling was evaluated for live cell imaging. Although higher concentrations of CHH were required (800 μmol/L), it was possible to reproduce carbonyl specific staining using PQ treated primary fibroblasts (Fig. S3).

The established DNPH staining provided in general a similar response in fluorescence as CHH labeling for PQ treated and untreated cells (Fig. 2), indicating that carbonylated species are mostly present in the cytoplasmic region but not in the nucleus. These data are in agreement with previous studies on DNPH immunocytochemistry in different cell types and under OS conditions [23,24]. To address the possible role of formaldehyde fixation (as carbonyl containing molecule) on background fluorescence intensity separate experiments using methanol fixation were performed (Fig. S4). No significant differences in background levels were observed between PFA and methanol fixation, thus all further experiments were performed using PFA.

Whereas the DNPH staining requires cell permeabilization, overnight DNPH labeling, intensive washing steps, incubations with primary and secondary antibodies, corresponding to at least 20 h of a total sample preparation time, CHH labeling can be accomplished within 3 h. Importantly, both staining techniques indicated a similar distribution of cellular carbonyls that increased in PQ treated primary fibroblasts (Fig. 2C and D). Close examination indicated distribution of carbonylated biomolecules in the cytoplasm and absence in the nuclear regions for both techniques (Fig. 3). The relative fluorescence intensities for CHH and DNPH labeling in the cytoplasmic regions were very similar, but CHH related signals were more intense in the perinuclear region of the cell. It is important to note, that in contrast to DNPH, CHH is lipophilic and can penetrate membranes and thus can react with both protein- and lipid-bound carbonyls (see below).

The versatility of CHH labeling in microscopy was further tested on other OS models. Rat primary cardiomyocytes challenged by peroxynitrite donor (SIN-1; 10 μmol/L) resulted in significantly increased carbonylation levels (Fig. S5). CHH staining was distributed in the cytoplasmic region and not in the nuclei, besides a strong perinuclear accumulation. Similarly, murine primary hepatocytes were treated with acetaminophen (10 mmol/L) which depletes the cellular glutathione, showed a strong increase of carbonyl specific fluorescence (Fig. S5) with the same spatial distribution of carbonylated molecules as described for the other two OS models.

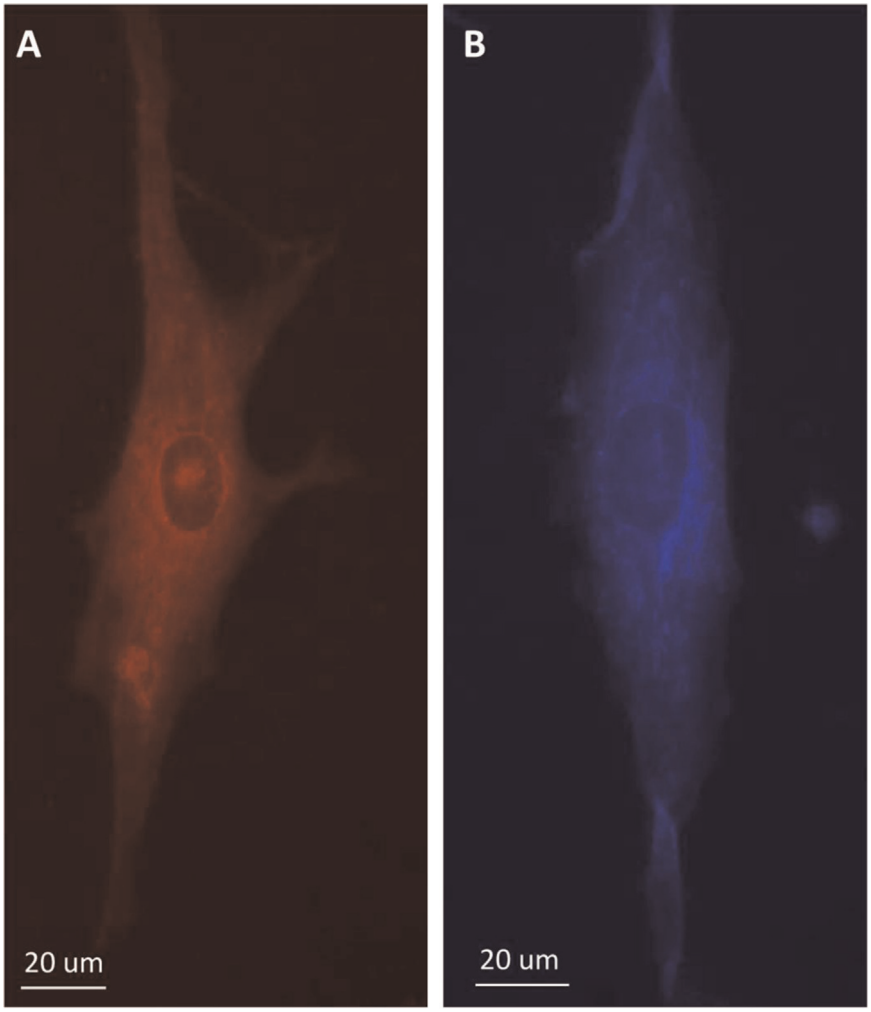

Fig. 3. Single cell fluorescence microscopy images of carbonyl stains obtained by DNPH-based immunocytochemistry (A) and chemical CHH labeling (B). Oxidative stress was induced with PQ (1 mmol/L, 1 h). Images are representatives of three independent experiments performed in triplicates.

CHH reactivity towards carbonylated biomolecules

Untreated and PQ-treated cells were collected and derivatized with CHH before lipids and proteins were separated by liquid–liquid extraction. The SDS-PAGE yielded several bands with significantly higher fluorescence intensity in PQ-treated samples than the corresponding bands of the control (Fig. S6). Conventional oxy-blot that rely on derivatization with DNPH after the protein transfer followed by an immunostaining, indicated similar levels of protein carbonylation (Fig. S6). Importantly, the carbonyl positive bands on CHH gels and DNPH blots were similar, especially for smaller proteins (below 40 kDa). The carbonyl-positive bands of the middle- and high-molecular weight proteins appeared more intense on the SDS-PAGE after CHH labeling than on the corresponding oxy-blots. Immunodetection of carbonylated proteins requires their transfer onto PVDF membrane and thus lower signal intensity for carbonylated proteins with higher molecular weight on the blots can be attributed to their lower blotting efficiencies compared to the low molecular weight proteins.

CHH labeled lipids obtained by liquid–liquid extraction were separated by NP HPTLC and visualized using fluorescence imaging (Fig. S6), to detect low molecular weight carbonylated lipids (aliphatic aldehydes and ketones such as alkanals, alkenals, and hydroxy-alkenals). CHH labeled propanal, heptanal, decanal as well as cholesterol (negative control) were used as standards (Fig. S6, line M) with R_f-values increasing with the length of the carbon chain. The cellular lipid samples indicated an accumulation of low molecular weight carbonyls in PQ-treated cells in comparison to control, as a primuline stain confirmed equal lipid loads for both control and PQ-treated samples based on the cholesterol band.

Recently we showed that CHH-labeling of oxidized lipids allows the simultaneous and sensitive detection and identification of both phospholipid-bound carbonyls and low molecular weight water soluble aliphatic aldehydes using ESI-MS/MS [18,27]. Additionally, CHH tertiary amino-group has a high proton affinity providing high ionization efficiencies of CHH-derivatized carbonylated lipids. CHH-derivatized lipids from control and PQ-treated cells were analyzed by shotgun lipidomics approach. Manual inspection of the tandem mass spectra identified CHH-derivatized lipid carbonyls, such as 4-hydroxy-nonenal (Fig. 4A), pentadecanal (Fig. 4B), 1-hydroxy-2-oxo-butanoyl-sn-glycero-3-

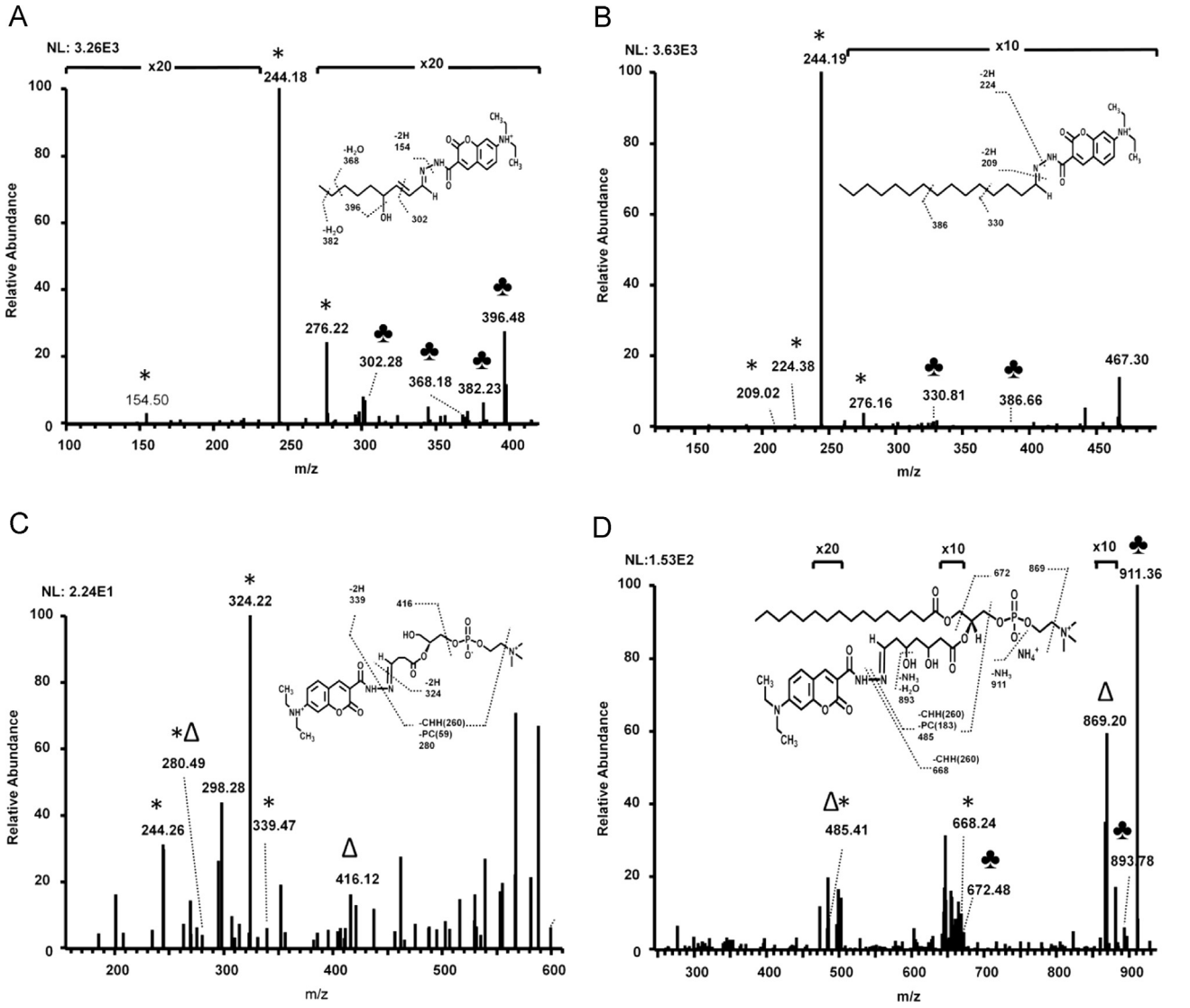

Fig. 4. CID tandem mass spectra of CHH-derivatized carbonylated lipids from cellular extracts of PQ-treated fibroblasts. CHH derivatized 4-hydroxy-2-nonenal (A), pentadecanal (B), 1-hydroxy-2-oxo-butanoyl-sn-glycero-3-phosphatidylcholine (C), and 1-palmitoyl-2-oxo-dihydroxy-heptanoyl-sn-glycero-3-phosphatidylcholine (D). CHH specific signals are marked by asterisks, lipid head group specific peaks are indicated by triangles and carbonylated phosphatidylcholine specific signals are marked by clovers.

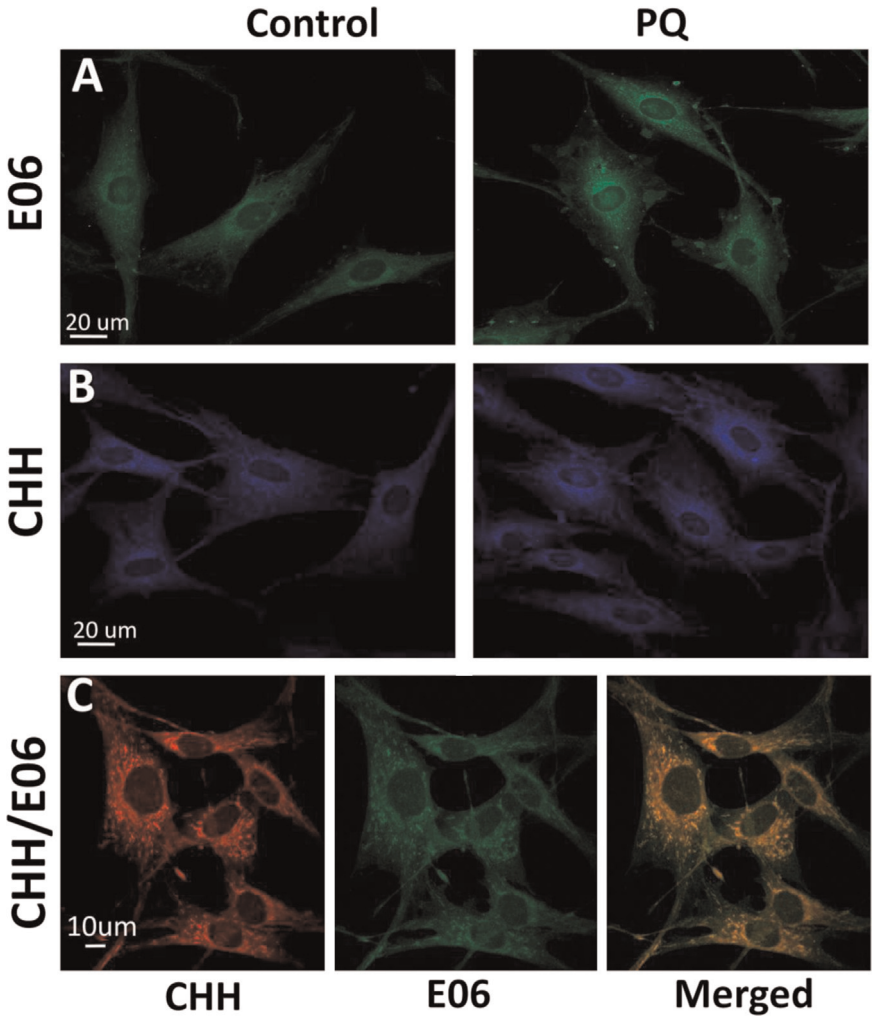

Fig. 5. Confocal fluorescence microscopy showing the subcellular localization of oxPL (A; control and PQ-treated) and carbonylated biomolecules (B; control and PQ-treated) alone or in co-staining experiments (C) in PQ-treated primary fibroblasts. Fixed cells were immunostained with E06 antibodies (green; A) and CHH (blue; B). For better representation of co-staining (C) E06 stain shown in green and CHH stain red colors. Merged images (yellow) demonstrate the co-localization of oxPL with carbonyl stain. Images are representatives of three independent experiments performed in triplicates.

phosphatidylcholine (Fig. 4C) and 1-palmitoyl-2-oxo-dihydroxy-heptanoyl-sn-glycero-3-phosphatidylcholine (Fig. 4D). This unambiguously illustrates the capability of CHH to label different types of lipid peroxidation products as well as variety of modified lipids formed by PQ treatment.

Fluorescent microscopy of oxidized phosphatidylcholines

Based on the detection of CHH-derivatized carbonylated phospholipids (oxPL) by MS, we evaluated oxPL subcellular distribution. To the best of our knowledge, the only immunocytochemical approach to detect oxidized phospholipids (oxPL) relies on natural Ab E06 recognizing oxidized phosphatidylcholines (oxPC). Though the exact epitope(s) are unknown, it recognizes oxidized fatty acids in *sn*-2 position and the PC head group. Fluorophore labeled Ab E06 indicated significantly increased amounts of oxPL in primary fibroblasts after PQ treatment (Fig. 5A). Interestingly, the images of many cells looked similar to the CHH staining (Fig. 5B), i.e. the oxPL specific fluorescence was mostly localized in the perinuclear space indicating that CHH labeling can localize carbonylated lipids. To confirm oxPL co-localization with carbonylated species, control and PQ-treated cells were used in co-staining experiments and imaged by confocal microscopy (Fig. 5C).

Discussion

Cellular carbonylation plays a vital role in many OS-related human disorders and its increase was correlated with disease progression. Carbonylation refers to a complex mixture of structurally diverse modifications in both proteins and lipids [11]. Detection of carbonylated biomolecules is usually done via labeling of carbonyl group by different chemical probes, including hydrazines (e.g. DNPH), hydrazides (e.g. biotin hydrazide and CHH) and hydroxylamines (aldehyde reactive probe and fluorescent hydroxylamine) [3]. Additionally, a number of antibodies raised against specific protein carbonyls are available, including antibodies against hydroxy-nonenal (HNE)- and malondialdehyde (MDA)-protein adducts [38–40]. In order to understand the dynamic behavior and the underlying mechanisms, it is crucial to identify and quantify carbonylated species as well as evaluate their spatial distribution in cells and tissues.

DNPH-based immunocytochemistry, as well as anti-HNE and anti-MDA Ab, are widely used to access spatial distribution of carbonylated proteins [40,41]. However, these protocols do not address lipid derived carbonyls. Further limitations of standard immunostaining protocols are permeabilization of cell plasma membranes and thin-sectioning of tissue samples in order to ensure antibody access to the targeted molecules. Additionally,

immunocytochemical protocols require cell fixation and thus are not suitable for live imaging. Finally, as for any antibody based techniques, specificity of antibodies is crucial.

Based on our recent studies on the favorable analysis of CHH labeled carbonylated lipids by mass spectrometry [18] we tested here this coumarin-hydrazide to detect carbonylated species by fluorescence microscopy in paraquat treated human primary fibroblasts. CHH is a versatile fluorescent chemical probe (λ_{ex} = 420–450/λ_{em}= 468 nm) with a characteristic blue light emission in the range of DAPI or Hoechst dyes. Generally, coumarin-based dyes have been favorably applied in numerous studies due to their high fluorescent efficiency, good solubility, and efficient cell permeability. In CHH the electron donating group in position 7 (N,N-diethyl group) and electron withdrawing group in position 3 (carbohydrazide) provide additionally high fluorescence quantum yields [42].

Samples reduced with sodium borohydride and thus missing reactive carbonyls indicated no unspecific background allowing time and dose dependent studies on PQ treated cells. Importantly, the fluorescence increased with both PQ concentration and incubation times. The fluorescence increased very fast within 15 min, reaching a maximum after 2 h before decreasing slightly due to the cell death. Thus CHH allows specific monitoring of the cellular carbonyls formation in response to external signals or reagents.

Microscopy imaging of total biomolecule carbonylation requires fixation protocols capable to preserve not only protein but also lipid, polysaccharide and nucleic structures within a cell. Fixation with paraformaldehyde (PFA) is widely used in cyto- and histochemistry studies. PFA, which is a formaldehyde polymer, might look like suboptimal choice of fixative for carbonyls detection. However, aqueous solution of PFA exists in equilibrium between methylene glycol and formaldehyde with a favor to methylene glycol [43]. Additionally it is important to note that formaldehyde can react with nucleophilic molecules (e.g. lysine primary amino group) only via Schiff base mechanism thus carbonyl function is consumed within the reaction and do not provide artificial levels of protein carbonylation. PFA fixation followed by hydrazide/hydrazine based detection of carbonylated biomolecules was used in multiple studies to address OS-related effects [44–48]. Application of organic solvent based fixatives (e.g. methanol, acetone) was shown to extract majority of cellular phospholipids and alter cellular structures with high lipid content (e.g. biological membranes, lipid droplets) [49] and thus would be unsuitable to study total biomolecules carbonylation. Furthermore, we did not observe significant differences in background fluorescence of PFA and methanol fixed cells stained with CHH. Thus PFA fixation which allow to preserve both protein and lipid cellular structures was used here to assess the total level of biomolecules carbonylation.

Gel electrophoresis of carbonylated proteins, TLC and MS of carbonylated lipids confirmed that CHH labels efficiently both carbonylated biomolecules. Gels can be directly used for fluorescent detection of carbonylated proteins without additional staining, which is also true for TLC separated carbonylated lipids. Finally, several molecular species of CHH-labeled carbonylated lipids, i.e. low molecular weight aliphatic aldehydes, lysoPC, and truncated PC species, were identified by MS.

Microscopy images obtained after CHH labeling and regular DNPH-based immunocytochemistry correlated well with CHH labeling being much faster (i.e. 3 versus 20 h), less expensive (no antibodies) and it simultaneously detects both protein and lipid derived carbonyls. The fluorescence imaging obtained by both techniques provided similar increases in cellular carbonyls indicating that both techniques allow quantitative evaluations.

Furthermore, specificity of hydrazine/hydrazide labeling reagents towards carbonyl groups in other biomolecules needs to be discussed. Free sugars (e.g. glucose) can carry carbonyl function but only in the open chain form. However, more than 99% of glucose is believed to be present in the cell in closed-ring form (pyranose) and thus will not be reactive to hydrazide tag. Glycoproteins might represent another source of OS-independent carbonyls. But similarly to free carbohydrates, sugar moieties in glycosylated proteins are present in the closed-ring form connected by glycosidic bonds.

Carbonyl groups in the nucleic acids, indeed, can be labeled by hydrazine. Reactivity of DNPH towards nucleic acids was reported by Luo and Wehr and streptomycin precipitation or enzymatic DNA/RNA degradation were proposed to be included in spectrophotometric DNPH-based protein carbonyl assays [16]. Thus it can be expected that coumarin-hydrazide will also be able to label carbonyl groups of nucleic acids. However, using DNPH and CHH for microscopy imaging we did not observe significant nuclear staining, as well as co-localization of DNPH- and CHH-signals with DNA specific dyes. DNA in the cell is not present in its linear form assessable to the labeling tag, but is folded in nucleosomes by histones and decorated by many other interacting proteins forming a compact chromatic structure. This can be one of the reasons why hydrazides/hydrazines do not show high reactivity towards cellular DNA in its native form. Overall, low level of carbonylation in cell nucleus was demonstrated on different cell types in a variety of oxidative stress models, and was attributed to the higher concentration of 20S proteasome in the nucleus as well as proteasome activation upon stress induction [50,51]. Indeed, the link between DNA repair mechanisms and activity of 20S proteasome was demonstrated via PARP-1-mediated proteasomal activation [52]. Furthermore, the role of nuclear glutathione (GSH) in maintaining low levels of DNA and protein damage upon oxidative stress was shown as well [53].

Previous studies demonstrated perinuclear accumulation of oxidized molecules in different models of OS, though this phenomena cannot be explained yet. Jung et al. concluded from the total and carbonylated protein distributions in HT-22 cells treated with different OS inducers that high carbonylation levels in perinuclear space correlate with high protein concentrations [23]. However, when protein carbonylation was normalized to the protein amounts along the cell space, the highest level of protein carbonyls was assigned to the cytosol near the plasma membrane. Recently, the high perinuclear clustering of HNE-modified proteins was attributed to protein carbonylation in the endoplasmic reticulum (ER) of rat aortic smooth muscle cells treated with HNE and several modified proteins including ER resident chaperons were identified by MS [40]. Our approach similarly indicated a strong perinuclear clustering of carbonylation specific signals in PQ-treated fibroblasts. Taking into account the lipophilic nature of CHH and TLC and MS data, we propose that these signals derived from both protein-bound carbonyls and carbonylated lipids formed under OS conditions. This was additionally confirmed by co-distribution of CHH signals with signals from natural antibodies E06 which localize oxidized lipids mainly around the nuclear membranes. The biological significance of low molecular weight aliphatic aldehydes is well known and was recently further extended for carbonylated phospholipids as inflammatory and immune responses modulators. However, the cellular and tissue distribution of carbonylated lipids are rarely studied. To the best of our knowledge, only one chemical probe, tetrazolium salt of 2-hydroxy-3-naphthoic acid hydrazide, was used to address this question [54]. Thus, ability of CHH to label both protein-bound and lipid derived carbonyls provides new opportunities to access the levels and spatial distribution of carbonylated species and can be further extended to tissue imaging experiments.

Conclusion

The present study demonstrates that 7-(diethylamino)-coumarin-3-carbohydrazide (CHH) is a time and cost efficient reagent for fluorescence microscopy imaging of carbonylated biomolecules in cellular models of OS. CHH labeling was equally efficient as conventional DNPH immunocytochemistry, but can be additionally combined with complimentary analytical techniques (SDS PAGE, TLC and MS) and fluorescence staining of oxidized phospholipids. We could prove that CHH stains protein-bound carbonyls and lipid-oxidation derived species, thus allowing to monitor subcellular distribution of a broad range of carbonylated biomolecules.

Acknowledgment

The authors are thankful to Dr. Tobias Jung and Prof. Tilman Grune (German Institute of Human Nutrition, Potsdam, Germany) for introduction to DNPH-based immunocytochemistry. We thank Prof. Ralf Hoffmann (Institute of Bioanalytical Chemistry, University of Leipzig) for providing access to his laboratory and mass spectrometers. The authors are also thankful to Prof. Thomas M. Magin (Division of Cell and Development Biology, Translational Centre for Regenerative Medicine and Biology, University of Leipzig) for providing access to confocal microscope. The financial support from Deutsche Forschungsgemeinschaft (DFG; FE-1236/3-1 to M.F.), European Regional Development Fund (ERDF, European Union and Free State Saxony; 100146238 and 100121468 to M.F) and COST Action CM1001 are gratefully acknowledged.

Appendix A. Supporting material

Supplementary data associated with this article can be found in the online version at http://dx.doi.org/10.1016/j.redox.2015.04.006.

References

[1] D.J. Betteridge, What is oxidative stress? Metabolism 49 (2) (2000) 3–8. http://dx.doi.org/10.1016/S0026-0495(00)80077-3.
[2] B. Halliwell, Oxidative stress and cancer: have we moved forward? Biochemical Journal 401 (1) (2007) 1–11. http://dx.doi.org/10.1042/BJ20061131 17150040.
[3] M. Fedorova, R.C. Bollineni, R. Hoffmann, Protein carbonylation as a major hallmark of oxidative damage: update of analytical strategies, Mass Spectrometry Reviews 33 (2) (2014) 79–97. http://dx.doi.org/10.1002/mas.21381 23832618.
[4] R. Ahmad, A.K. Tripathi, P. Tripathi, S. Singh, R. Singh, R.K. Singh, Malondialdehyde and protein carbonyl as biomarkers for oxidative stress and disease progression in patients with chronic myeloid leukemia, In Vivo 22 (4) (2008) 525–528 18712183.
[5] A. Castegna, M. Aksenov, V. Thongboonkerd, J.B. Klein, W.M. Pierce, R. Booze, W.R. Markesbery, D.A. Butterfield, Proteomic identification of oxidatively modified proteins in Alzheimer's disease brain. Part II: Dihydropyrimidinase-related protein 2, alpha-enolase and heat shock cognate 71, Journal of Neurochemistry 82 (6) (2002) 1524–1532. http://dx.doi.org/10.1046/j.1471-4159.2002.01103.x 12354300.
[6] C. Domínguez, E. Ruiz, M. Gussinye, A. Carrascosa, Oxidative stress at onset and in early stages of type 1 diabetes in children and adolescents, Diabetes Care 21 (10) (1998) 1736–1742. http://dx.doi.org/10.2337/diacare.21.10.1736 9773740.
[7] E. Floor, M.G. Wetzel, Increased protein oxidation in human substantia nigra pars compacta in comparison with basal ganglia and prefrontal cortex measured with an improved dinitrophenylhydrazine assay, Journal of Neurochemistry 70 (1) (1998) 268–275. http://dx.doi.org/10.1046/j.1471-4159.1998.70010268.x 9422371.
[8] I. Dalle-Donne, R. Rossi, D. Giustarini, A. Milzani, R. Colombo, Protein carbonyl groups as biomarkers of oxidative stress, Clinica Chimica Acta 329 (1–2) (2003) 23–38. http://dx.doi.org/10.1016/S0009-8981(03)00003-2 12589963.
[9] Y.J. Suzuki, M. Carini, D.A. Butterfield, Protein carbonylation, Antioxidants & Redox Signaling 12 (3) (2010) 323–325. http://dx.doi.org/10.1089/ars.2009.2887.
[10] L. Lyras, R.H. Perry, E.K. Perry, P.G. Ince, A. Jenner, P. Jenner, B. Halliwell, Oxidative damage to proteins, lipids, and DNA in cortical brain regions from patients with dementia with Lewy bodies, Journal of Neurochemistry 71 (1) (1998) 302–312. http://dx.doi.org/10.1046/j.1471-4159.1998.71010302.x 9648879.
[11] I. Dalle-Donne, G. Aldini, M. Carini, R. Colombo, R. Rossi, A. Milzani, Protein carbonylation, cellular dysfunction, and disease progression, Journal of Cellular and Molecular Medicine 10 (2) (2006) 389–406. http://dx.doi.org/10.1111/j.1582-4934.2006.tb00407.x 16796807.
[12] F.H. Greig, S. Kennedy, C.M. Spickett, Physiological effects of oxidized phospholipids and their cellular signaling mechanisms in inflammation, Free Radical Biology and Medicine 52 (2) (2012) 266–280. http://dx.doi.org/10.1016/j.freeradbiomed.2011.10.481 22080084.
[13] L.J. Yan, M.J. Forster, Chemical probes for analysis of carbonylated proteins: a review, Journal of Chromatography B: Analytical Technologies in the Biomedical and Life Sciences 879 (17–18) (2011) 1308–1315. http://dx.doi.org/10.1016/j.jchromb.2010.08.004 20732835.
[14] R.L. Levine, D. Garland, C.N. Oliver, A. Amici, I. Climent, A.G. Lenz, B.W. Ahn, S. Shaltiel, E.R. Stadtman, Determination of carbonyl content in oxidatively modified proteins, Methods in Enzymology 186 (1990) 464–478. http://dx.doi.org/10.1016/0076-6879(90)86141-H 1978225.
[15] H. Uehara, V.A. Rao, Metal-mediated protein oxidation: applications of a modified ELISA-Based carbonyl detection assay for complex proteins, Pharmaceutical Research 32 (2015) 691–701. http://dx.doi.org/10.1007/s11095-014-1496-y 25182973.
[16] S. Luo, N.B. Wehr, Protein carbonylation: avoiding pitfalls in the 2,4-dinitrophenylhydrazine assay, Redox Report 14 (4) (2009) 159–166. http://dx.doi.org/10.1179/135100009X392601 19695123.
[17] J.M. Anderson, Fluorescent hydrazides for the high-performance liquid chromatographic determination of biological carbonyls, Analytical Biochemistry 152 (1) (1986) 146–153. http://dx.doi.org/10.1016/0003-2697(86)90133-8 2937341.
[18] I. Milic, R. Hoffmann, M. Fedorova, Simultaneous detection of low and high molecular weight carbonylated compounds derived from lipid peroxidation by electrospray ionization-tandem mass spectrometry, Analytical Chemistry 85 (1) (2013) 156–162. http://dx.doi.org/10.1021/ac302356z 23186270.
[19] R.C. Bollineni, M. Fedorova, M. Blüher, R. Hoffmann, Carbonylated plasma proteins as potential biomarkers of obesity induced type 2 diabetes mellitus, Journal of Proteome Research 13 (11) (2014) 5081–5093. http://dx.doi.org/10.1021/pr500324y 25010493.
[20] M.E. Harris, J.M. Carney, D.H. Hua, R.A. Leedle, Detection of oxidation products in individual neurons by fluorescence microscopy, Experimental Neurology 129 (1) (1994) 95–102. http://dx.doi.org/10.1006/exnr.1994.1150 7925846.
[21] V. Kostal, K. Levar, M. Swift, E. Skillrud, M. Chapman, L.V. Thompson, E. A. Arriaga, Semi-automated image analysis: detecting carbonylation in subcellular regions of skeletal muscle, Analytical and Bioanalytical Chemistry 400 (1) (2011) 213–222. http://dx.doi.org/10.1007/s00216-011-4725-9 21327623.
[22] J. Feng, M. Navratil, L.V. Thompson, E.A. Arriaga, Estimating relative carbonyl levels in muscle microstructures by fluorescence imaging, Anal. Bioanal. Chem. 391 (7) (2008) 2591–2598. http://dx.doi.org/10.1007/s00216-008-2187-5 18548236.
[23] T. Jung, M. Engels, B. Kaiser, D. Poppek, T. Grune, Intracellular distribution of oxidized proteins and proteasome in HT22 cells during oxidative stress, Free Radical Biology and Medicine 40 (8) (2006) 1303–1312. http://dx.doi.org/10.1016/j.freeradbiomed.2005.11.023 16631520.
[24] T. Jung, M. Engels, L.O. Klotz, K.D. Kröncke, T. Grune, Nitrotyrosine and protein carbonyls are equally distributed in HT22 cells after nitrosative stress, Free Radical Biology and Medicine 42 (6) (2007) 773–786. http://dx.doi.org/10.1016/j.freeradbiomed.2006.11.029 17320760.
[25] T. Jung, A. Höhn, B. Catalgol, T. Grune, Age-related differences in oxidative protein-damage in young and senescent fibroblasts, Archives of Biochemistry and Biophysics 483 (1) (2009) 127–135. http://dx.doi.org/10.1016/j.abb.2008.12.007 19135972.
[26] M.A. Smith, L.M. Sayre, V.E. Anderson, P.L. Harris, M.F. Beal, N. Kowall, G. Perry, Cytochemical demonstration of oxidative damage in Alzheimer disease by immunochemical enhancement of the carbonyl reaction with 2,4-dinitrophenylhydrazine, J. Histochem. Cytochem. 46 (6) (1998) 731–735. http://dx.doi.org/10.1177/002215549804600605 9603784.
[27] I. Milic, M. Fedorova, Derivatization and detection of small aliphatic and lipid-bound carbonylated lipid peroxidation products by ESI-MS, Methods in Molecular Biology 1208 (2015) 3–20. http://dx.doi.org/10.1007/978-1-4939-1441-8_1 25323495.
[28] W. Palinski, S. Hörkkö, E. Miller, U.P. Steinbrecher, H.C. Powell, L.K. Curtiss, J. L. Witztum, Cloning of monoclonal autoantibodies to epitopes of oxidized lipoproteins from apolipoprotein E-deficient mice. Demonstration of epitopes of oxidized low density lipoprotein in human plasma, Journal of Clinical Investigation 98 (3) (1996) 800–814. http://dx.doi.org/10.1172/JCI118853 8698873.
[29] M.K. Chang, C. Bergmark, A. Laurila, S. Hörkkö, K.H. Han, P. Friedman, E. A. Dennis, J.L. Witztum, Monoclonal antibodies against oxidized low-density lipoprotein bind to apoptotic cells and inhibit their phagocytosis by elicited macrophages: evidence that oxidation-specific epitopes mediate macrophage recognition, Proceedings of the National Academy of Sciences of the United

States of America 96 (11) (1999) 6353–6358. http://dx.doi.org/10.1073/pnas.96.11.6353 10339591.
[30] V. Matyash, G. Liebisch, T.V. Kurzchalia, A. Shevchenko, D. Schwudke, Lipid extraction by methyl-tert-butyl ether for high-throughput lipidomics, Journal of Lipid Research 49 (5) (2008) 1137–1146. http://dx.doi.org/10.1194/jlr.D700041-JLR200 18281723.
[31] B.J. Day, M. Patel, L. Calavetta, L.Y. Chang, J.S. Stamler, A mechanism of paraquat toxicity involving nitric oxide synthase, Proceedings of the National Academy of Sciences of the United States of America 96 (22) (1999) 12760–12765. http://dx.doi.org/10.1073/pnas.96.22.12760 10535996.
[32] T. Fukushima, K. Tanaka, H. Lim, M. Moriyama, Mechanism of cytotoxicity of paraquat, Environmental Health and Preventive Medicine 7 (3) (2002) 89–94. http://dx.doi.org/10.1265/ehpm.2002.89 21432289.
[33] B.J. Day, S. Shawen, S.I. Liochev, J.D. Crapo, A metalloporphyrin superoxide dismutase mimetic protects against paraquat-induced endothelial cell injury, in vitro, Journal of Pharmacology and Experimental Therapeutics 275 (3) (1995) 1227–1232 8531085.
[34] J. Krall, A.C. Bagley, G.T. Mullenbach, R.A. Hallewell, R.E. Lynch, Superoxide mediates the toxicity of paraquat for cultured mammalian cells, Journal of Biological Chemistry 263 (4) (1988) 1910–1914 2828357.
[35] D.K. St Clair, T.D. Oberley, Y.S. Ho, Overproduction of human Mn-superoxide dismutase modulates paraquat-mediated toxicity in mammalian cells, FEBS Letters 293 (1–2) (1991) 199–203. http://dx.doi.org/10.1016/0014-5793(91)81186-C 1959661.
[36] M. Tsukamoto, Y. Tampo, M. Sawada, M. Yonaha, Paraquat-induced oxidative stress and dysfunction of the glutathione redox cycle in pulmonary microvascular endothelial cells, Toxicology and Applied Pharmacology 178 (2) (2002) 82–92. http://dx.doi.org/10.1006/taap.2001.9325 11814328.
[37] A.C. Cristóvão, D.H. Choi, G. Baltazar, M.F. Beal, Y.S. Kim, The role of NADPH oxidase 1-derived reactive oxygen species in paraquat-mediated dopaminergic cell death, Antioxidants & Redox Signaling 11 (9) (2009) 2105–2118. http://dx.doi.org/10.1089/ARS.2009.2459 19450058.
[38] E. Kurisaki, K. Hiraiwa, Western blot analysis for 4-hydroxy-2-nonenal (HNE)-modified proteins in paraquat-treated mice, Legal Medicine (Tokyo) 11 (Suppl. 1) (2009) S431–S433. http://dx.doi.org/10.1016/j.legalmed.2009.01.082 19261533.
[39] V. Nobili, M. Parola, A. Alisi, F. Marra, F. Piemonte, C. Mombello, S. Sutti, D. Povero, V. Maina, E. Novo, E. Albano, Oxidative stress parameters in paediatric non-alcoholic fatty liver disease, International Journal of Molecular Medicine 26 (4) (2010) 471–476. http://dx.doi.org/10.3892/ijmm_00000487 20818484.
[40] P. Haberzettl, B.G. Hill, Oxidized lipids activate autophagy in a JNK-dependent manner by stimulating the endoplasmic reticulum stress response, Redox Biology 1 (2013) 56–64. http://dx.doi.org/10.1016/j.redox.2012.10.003 24024137.
[41] T. Hirao, M. Takahashi, Carbonylation of cornified envelopes in the stratum corneum, FEBS Letters 579 (30) (2005) 6870–6874. http://dx.doi.org/10.1016/j.febslet.2005.11.032 16336969.
[42] H. Takechi, Y. Oda, N. Nishizono, K. Oda, M. Machida, Screening search for organic fluorophores: syntheses and fluorescence properties of 3-azolyl-7-diethylaminocoumarin derivatives, Chemical & Pharmaceutical Bulletin 48 (11) (2000) 1702–1710. http://dx.doi.org/10.1248/cpb.48.1702 11086899.
[43] R. Thavarajah, V.K. Mudimbaimannar, J. Elizabeth, U.K. Rao, K. Ranganathan, Chemical and physical basics of routine formaldehyde fixation, Journal of Oral and Maxillofacial Pathology 16 (3) (2012) 400–405. http://dx.doi.org/10.4103/0973-029X.102496 23248474.
[44] A. Oberbach, N. Schlichting, M. Heinrich, H. Till, J.U. Stolzenburg, J. Neuhaus, Free fatty acid palmitate impairs the vitality and function of cultured human bladder smooth muscle cells, PLOS One 7 (7) (2012) e41026. http://dx.doi.org/10.1371/journal.pone.0041026 22808290.
[45] G. Colombo, I. Dalle-Donne, M. Orioli, D. Giustarini, R. Rossi, M. Clerici, L. Regazzoni, G. Aldini, A. Milzani, D.A. Butterfield, N. Gagliano, Oxidative damage in human gingival fibroblasts exposed to cigarette smoke, Free Radical Biology and Medicine 52 (9) (2012) 1584–1596. http://dx.doi.org/10.1016/j.freeradbiomed.2012.02.030 22387198.
[46] Z. Zhang, N.I. Dmitrieva, J.-H. Park, R.L. Levine, M.B. Burg, High urea and NaCl carbonylate proteins in renal cells in culture and in vivo, and high urea causes 8-oxoguanine lesions in their DNA, Proceedings of the National Academy of Sciences of the United States of America 101 (25) (2004) 9491–9496. http://dx.doi.org/10.1073/pnas.0402961101 15190183.
[47] R.C. Lazarus, J.E. Buonora, D.M. Jacobowitz, G.P. Mueller, Protein carbonylation after traumatic brain injury: cell specificity, regional susceptibility, and gender differences, Free Radical Biology and Medicine 78 (2015) 89–100. http://dx.doi.org/10.1016/j.freeradbiomed.2014.10.507 25462645.
[48] A. Dasgupta, J. Zheng, O.A. Bizzozero, Protein carbonylation and aggregation precede neuronal apoptosis induced by partial glutathione depletion, ASN Neuro 4 (2012) 161–174.
[49] D. DiDonato, D.L. Brasaemle, Fixation methods for the study of lipid droplets by immunofluorescence microscopy, Journal of Histochemistry & Cytochemistry 51 (6) (2003) 773–780. http://dx.doi.org/10.1177/002215540305100608.
[50] T.J. Höhn, T. Grune, The proteasome and the degradation of oxidized proteins: Part III-Redox regulation of the proteasomal system, Redox Biology 2 (2014) 388–394. http://dx.doi.org/10.1016/j.redox.2013.12.029 24563857.
[51] T. Jung, A. Höhn, T. Grune, The proteasome and the degradation of oxidized proteins: Part II – protein oxidation and proteasomal degradation, Redox Biology 2C (2013) 99–104. http://dx.doi.org/10.1016/j.redox.2013.12.008 25460724.
[52] E. Bakondi, B. Catalgol, I. Bak, T. Jung, P. Bozaykut, M. Bayramicli, N.K. Ozer, T. Grune, Age-related loss of stress-induced nuclear proteasome activation is due to low PARP-1 activity, Free Radical Biology and Medicine 50 (1) (2011) 86–92. http://dx.doi.org/10.1016/j.freeradbiomed.2010.10.700 20977936.
[53] E. Hatem, V. Berthonaud, M. Dardalhon, G. Lagniel, P. Baudouin-Cornu, M. E. Huang, J. Labarre, S. Chédin, Glutathione is essential to preserve nuclear function and cell survival under oxidative stress, Free Radical Biology and Medicine 67 (2014) 103–114. http://dx.doi.org/10.1016/j.freeradbiomed.2013.10.807 24145121.
[54] A. Pompella, M. Comporti, Imaging of oxidative stress at subcellular level by confocal laser scanning microscopy after fluorescent derivatization of cellular carbonyls, American Journal of Pathology 142 (5) (1993) 1353–1357 8494040.